Structural and Magnetic Characterization of Co and Ni Silicate Hydroxides in Bulk and in Nanostructures within Silica Aerogels

Daniela Carta,[†] Maria F. Casula,[†] Anna Corrias,[*,†] Andrea Falqui,[†] Danilo Loche,[†]
Gavin Mountjoy,[†,‡] and Peng Wang[§]

Dipartimento di Scienze Chimiche and INSTM, Università di Cagliari, S.S. 554 bivio per Sestu, I-09042 Monserrato, Cagliari, Italy, and SuperSTEM, Daresbury Laboratory, Keckwick Lane, Daresbury, Cheshire WA4 4AD, United Kingdom

Received October 31, 2008. Revised Manuscript Received December 22, 2008

X-ray diffraction, transmission electron microscopy, X-ray absorption spectroscopy, and magnetic measurements were used to investigate highly porous silica aerogels containing iron and cobalt or iron and nickel, calcined at 450 °C, which are intermediates in the formation of $CoFe_2O_4-SiO_2$ and $NiFe_2O_4-SiO_2$ aerogel nanocomposites. Aerogels without iron and pure Co and Ni silicate hydroxides were also studied. The aerogel samples containing iron and cobalt or iron and nickel present two separate phases, one containing iron in the form of ferrihydrite and the other either Co or Ni silicate hydroxides. The silicate hydroxides are present in the aerogels in form of nanoparticles with a one-dimensional appearance in electron microscopy images, which are therefore anisotropic nanostructures, such as nanoneedles or nanosheets. The study of the magnetic properties indicates that the coercivity is greatly modified by size and shape of the particles going from pure Co or Ni silicate hydroxides to the aerogel samples containing only nickel or only cobalt. Finally, in the samples also containing iron, the total magnetic behavior is influenced both by the presence of ferrihydrite and by the possible diffusion of iron in the nanostructures of cobalt or nickel silicate hydroxide.

1. Introduction

Metal and metal oxide nanocomposites play a key role in heterogeneous catalysis as well as in electronic and magnetic device fabrication.[1−3] The properties of these materials can be targeted by finely tuning particle size and shape, particle−support interactions, dispersion degree of the nanoparticles within the matrix, and texture of the matrix.[4−6] Because of its high transparency, low dielectric constant, relative thermal stability, and chemical inertness, silica is widely used as a matrix. In addition, through well-developed sol−gel routes, the desired porous texture with controlled pore size and shape can be obtained and extremely high porosity, such as in aerogels, can be achieved.[7] Typical approaches for the preparation of silica-based nanocomposites include deposition−precipitation routes, pore volume impregnation, and cogelation.

In all these approaches, the final dispersed metal/metal oxide nanocrystals are formed upon post synthesis treatments, such as calcination under controlled atmosphere. The detailed mechanism and the intermediate species that give rise to the final nanocomposite are often misinterpreted or not fully understood because of the difficulties in the characterization of poorly ordered and nonstoichiometic phases. This issue limits the control over the preparation of nanocomposites, as the phases present at early stages deeply affect the final outcome of the synthesis. Moreover, the study of such phases will help elucidate the structure and peculiar properties of species which are commonly found and neglected in many hydrolytic processes (including soil science).

We have recently developed a urea-assisted sol−gel method[8] to produce highly porous $CoFe_2O_4-SiO_2$ nanocomposite aerogels. Suitable precursors are mixed in solution (sol) and aerogels are obtained by supercritical drying of the gels. The aerogels thus obtained are submitted to further thermal treatments up to 900 °C in order to obtain the final nanocomposites. The method is of general applicability for supported ferrites and has been extended to other magnetic aerogel nanocomposites, such as $FeCo-SiO_2$.[9]

Although the structure of the final nanocomposite aerogels has been thoroughly elucidated through the complementary use of several techniques, the study of the aerogel just after supercritical drying and after the first calcination at 450 °C

---

[*] To whom correspondence should be addressed. E-mail: corrias@unica.it.

[†] Università di Cagliari.

[‡] Permanent address: School of Physical Sciences, Ingram Building, University of Kent, Canterbury CT2 7NH, United Kingdom.

[§] Daresbury Laboratory.

(1) Yi, D. K.; Lee, S. S.; Ying, J. Y. *Chem. Mater.* **2006**, *18*, 2459.

(2) Buchanan, K. S.; Zhu, X.; Meldrum, A.; Freeman, M. R. *Nano Lett.* **2005**, *5*, 383.

(3) Haque, S. A.; Koops, S.; Tokmoldin, N.; Durrant, J. R.; Huang, J. S.; Bradley, D. D. C.; Palomares, E. *Adv. Mater.* **2007**, *19*, 683.

(4) Yang, C.-M.; Lin, H.-A.; Zibrowius, B.; Spliethoff, B.; Schuth, F.; Liou, S.-C.; Chu, M.-W.; Chen, C.-H. *Chem. Mater.* **2007**, *19*, 3205.

(5) Mohanan, J. L.; Brock, S. L. *Chem. Mater.* **2003**, *15*, 2567.

(6) Gross, A. F.; Diehl, M. R.; Beverly, K. C.; Richman, E. K.; Tolbert, S. H. *J. Phys. Chem. B* **2003**, *107*, 5475.

(7) Schubert, U.; Husing, N. In *Synthesis of Inorganic Materials*; Wiley-VCH: Weinheim, Germany, 2000; Chapter 6.

(8) Casula, M. F.; Loche, D.; Marras, S.; Paschina, G.; Corrias, A. *Langmuir* **2007**, *23*, 3509.

(9) Casu, A.; Casula, M. F.; Corrias, A.; Falqui, A.; Loche, D.; Marras, S.; Sangregorio, C. *Phys. Chem. Chem. Phys.* **2008**, *10*, 1043.

10.1021/cm8029714 CCC: $40.75

turned out to be quite difficult because the phases present at this stage have poor crystallinity and are dispersed in the silica matrix, the latter accounting for 90% of the sample. Nevertheless, evidence was found of the presence of two separate dispersed phases:[10,11] one containing Fe, which has been quite definitely identified as a poorly crystalline iron oxide hydroxide called ferrihydrite, and one containing Co (or Ni), which was suggested to have some resemblance to phyllosilicate hydroxide compounds.

Silicate hydroxides are very interesting materials, and in recent years they have been the subject of research for their potential in many areas, such as catalysis, absorption, and magnetic applications.[12] In particular, cobalt and nickel silicate hydroxide nanoparticles have recently attracted attention for their remarkable electrochemical[13] and magnetic[14] properties, respectively. The formation of cobalt silicate hydroxides and nickel silicate hydroxides was observed in the coprecipitation of Co(II) and Ni(II) nitrate with silica or by adsorption of Co(II) and Ni(II) on a silica surface.[15] These compounds usually have a phyllosilicate structure, which is a layered structure formed by sheets of tetrahedral silicon (surrounded by 4 oxygens) and sheets of octahedral Co(II) and Ni(II) cations (surrounded by 6 oxygens).[16]

In this paper, we provide clear evidence of the formation of cobalt and nickel silicate hydroxide, in the form of nanoneedles (acicular nanoparticles) or nanosheets, during the first stages of the thermal treatment of the nanocomposites aerogels. To obtain this evidence, we have characterized the structure and the magnetic properties of the aerogels calcined at 450 °C in detail and compared them with those of pure cobalt and nickel silicate hydroxides, which were prepared as reference compounds.

To perform such a thorough characterization, we combined several experimental techniques. X-ray diffraction (XRD) is used to gather some first indications on the phases that are present. Transmission electron microscopy (TEM) is used to characterize the morphology of the samples, and high-resolution scanning transmission electron microscopy (STEM) has been used to reveal a layered structure within anisotropic nanostructures. More detailed structural information is obtained by X-ray absorption spectroscopy. In fact, EXAFS (extended X-ray absorption fine structure) and XANES (X-ray absorption near edge structure) are very powerful tools for the structural study of nanoparticles dispersed in an amorphous matrix[10,11,17−24] Because these techniques are element specific and sensitive to the local structure,[25] they are ideal for studying multicomponent dilute and disordered materials. Moreover, these techniques can be used to distinguish Co/Ni silicate hydroxides from Co/Ni hydroxides, which have a similar layered structure and cannot therefore be easily distinguished by using conventional X-ray diffraction.[26−28] The characterization of the samples is completed by performing magnetic measurements.

There are very few reports about cobalt and nickel silicate hydroxide nanoparticles, especially embedded in a silica matrix. In particular, to the best of the authors' knowledge, this is the first time the magnetic properties of these systems are presented.

2. Experimental Section

2.1. Synthesis. The aerogel samples investigated in the present study are intermediates in the synthesis of highly porous $CoFe_2O_4-SiO_2$ and $NiFe_2O_4-SiO_2$ nanocomposites.[8] The synthesis is carried out by sol−gel process using tetraethoxysilane ($(Si(OC_2H_5)_4$, Aldrich 98%, TEOS) as a precursor for silica, iron(III), and cobalt(II) or nickel(II) nitrates ($Fe(NO_3)_3 \cdot 9H_2O$, Aldrich, 98%, $Co(NO_3)_2 \cdot 6H_2O$, $Ni(NO_3)_2 \cdot 6H_2O$ Aldrich, 98%) as precursors for the cobalt and nickel ferrite nanoparticles, respectively, which in the final nanocomposites are dispersed in the silica matrix, and absolute ethanol (EtOH, Fluka) as mutual solvent.[8] The precursors were added in such a way to obtain final nanocomposites containing a nominal ratio of 10 wt % $CoFe_2O_4/(CoFe_2O_4+SiO_2)$ and $NiFe_2O_4/(NiFe_2O_4+SiO_2)$. The ethanolic solution of the metal salts was added into the prehydrolyzed TEOS under acidic catalysis. Urea (NH_2CONH_2, Aldrich, >99.0%) was then added under reflux for 2 h at 85 °C as basic gelation agent. The sols were left in a closed container at 40 °C; gelation occurred in less than 2 days. The alcogels were submitted to high-temperature supercritical drying in an autoclave (Parr, 300 cm^3). The autoclave was filled with an appropriate amount of ethanol and flushed with N_2 before being heated in such a way to take the solvent to the supercritical state (i.e., 330 °C, 70 atm). The autoclave was then vented and highly porous aerogel samples were obtained. The samples investigated in the present study were then calcined at 450 °C for 1 h, whereas in order to obtain the final $CoFe_2O_4-SiO_2$ and $NiFe_2O_4-SiO_2$ nanocomposites, additional calcination up to 900 °C is required.

The two aerogels calcined at 450 °C will be hereafter called AFeCo_450 and AFeNi_450, respectively. To distinguish the presence of Fe, Co, and Ni intermediate phases, three other aerogels

---

(10) Carta, D.; Mountjoy, G.; Navarra, G.; Casula, M. F.; Loche, D.; Marras, S.; Corrias, A. *J. Phys. Chem. C* **2007**, *111*, 6308.
(11) Carta, D.; Loche, D.; Mountjoy, G.; Navarra, G.; Corrias, A. *J. Phys. Chem. C* **2008**, *112*, 15623.
(12) Richard-Plouet, M.; Vilminot, S.; Guillot, M.; Kurmoo, M. *Chem. Mater.* **2002**, *14*, 3829.
(13) Zhang, G.-Q.; Zhao, Y-Q.; Tao, F.; Li, H.-L. *J. Power Sources* **2006**, *161*, 723.
(14) Richard-Plouet, M.; Vilminot, S. *J. Mater. Chem.* **1998**, *8*, 131.
(15) Charlet, L.; Manceau, A. *Geochim. Cosmochim. Acta* **1994**, *58*, 2577.
(16) Kloprogge, J. T.; Hammond, M.; Hickey, L.; Frost, R. L. *J. Mater. Sci. Lett.* **2002**, *21*, 931.
(17) Corrias, A.; Casula, M. F.; Ennas, G.; Marras, S.; Navarra, G.; Mountjoy, G. *J. Phys. Chem. B* **2003**, *107*, 3030.
(18) Corrias, A.; Navarra, G.; Casula, M. F.; Marras, S.; Mountjoy, G. *J. Phys. Chem. B* **2005**, *109*, 13964.
(19) Carta, D.; Mountjoy, G.; Gass, M.; Navarra, G.; Casula, M. F.; Corrias, A. *J. Chem. Phys.* **2007**, *127*, 204705.
(20) Araujo, L. L.; Kluth, P.; Azevedo, G. D. M.; Ridgway, M. C. *Phys. Rev. B* **2006**, *74*, 184102.
(21) Grandjean, D.; Benfield, R. E.; Nayral, C.; Maisonnat, A.; Chaudret, B. *J. Phys. Chem. B* **2004**, *108*, 8876.
(22) Kluth, P.; Johannessen, B.; Foran, G. J.; Cookson, D. J.; Kluth, S. M.; Ridgway, M. C. *Phys. Rev. B* **2006**, *74*, 014202.
(23) Nishi, N.; Kosugi, K.; Hino, K.; Yokoyama, T. *Eur. Phys. J. D* **2003**, *24*, 97.
(24) Prestipino, C.; Bordiga, S.; Lamberti, C.; Vidotto, S.; Garilli, M.; Cremaschi, B.; Marsella, A.; Leofanti, G.; Fisicaro, P.; Spoto, G.; Zecchina, A. *J. Phys. Chem. B* **2003**, *107*, 5022.
(25) Koningsberger, D. C.; Prins, R. *X-ray Absorption. Principles, Applications, Techniques of EXAFS, SEXAFS and XANES*; Wiley: New York, 1988.
(26) Manceau, A.; Schlegel, M.; Nagy, K. L.; Charlet, L. *J. Colloid Interface Sci.* **1999**, *220*, 181.
(27) Manceau, A. *Can. Mineral.* **1990**, *28*, 321.
(28) Scheinost, A. C.; Sparks, D. L. *J. Colloid Interface Sci.* **2000**, *223*, 167.

were also prepared with the same procedure and calcined at 450 °C for 1 h, two of which do not contain Fe and one containing only Fe (in this case, the precursors were added in such a way to obtain final nanocomposites containing a nominal ratio of about 10 wt % Co_3O_4/(Co_3O_4+SiO_2), NiO/(NiO+SiO_2), and Fe_3O_4/(Fe_3O_4+SiO_2). These samples will be hereafter called ACo_450, ANi_450, and AFe_450, respectively.

Pure cobalt silicate hydroxide and nickel silicate hydroxide to be used as reference compounds were also synthesized using the route described in ref 29. Briefly, 8 mL of a 0.1 M solution of Na_2SiO_3 (Alfa Aesar) was added to 2 mL of a 0.3 M solution of anhydrous $CoCl_2$ (Aldrich, 97%) or anhydrous $NiCl_2$ (Alfa Aesar, 98%) in the presence of 0.4 mL of a 1 M solution of HCl. The precipitates obtained were washed with distilled water. After being dispersed in 500 mL of distilled water, the precipitates were left in a covered beaker at 75 °C for 2 weeks and then filtered and dried in an oven at 40 °C.

2.2. Characterization. XRD patterns were recorded on a X3000 Seifert diffractometer equipped with a graphite monochromator on the diffracted beam. The scans were collected within the range of 7−70° (2θ) using Cu Kα radiation.

TEM micrographs were recorded on a JEOL 200CX microscope operating at 200 kV. High resolution STEM images were recorded on a VG501 STEM microscope operating at 100 kV, equipped with a cold field emission gun and a spherical aberration corrector giving a very small 0.13 nm diameter probe (located at SuperSTEM, Daresbury Laboratory, Daresbury, U.K.). The samples for microscopy were dispersed in ethanol and dropped onto carbon-coated copper grids.

EXAFS and XANES spectra were recorded in transmission mode at beamline 11.1 (XAFS) at the ELETTRA synchrotron (Trieste, Italy). Spectra at the Co (7709 eV) and Ni (8333 eV) K-edges were acquired at room temperature using a Si(111) monochromator. The energy calibration was confirmed to be highly stable (to ±0.2 eV) by measuring the energy of the first inflection point in reference spectra of Fe, Co, and Ni metal foils. Data were collected on AFeCo_450, AFeNi_450, ACo_450, and ANi_450 and on the cobalt silicate hydroxide and nickel silicate hydroxide reference compounds. Samples with a suitable and highly uniform optical thickness were prepared from powders. In the case of the reference samples, the powders were dispersed in an inert solvent and then filtered onto polyethylene supports. The aerogel samples were pressed into a cardboard frame with mylar windows without the need to use any dispersing agent, the aerogels being very easy to compress because of their very low apparent density.

Measurements of static magnetic susceptibilities were performed on a Quantum Design MPMS-5XL squid magnetometer equipped with a superconducting magnet producing fields up to 5 T. Zero-field-cooled (ZFC) magnetizations were measured by cooling the samples in a zero magnetic field and then increasing the temperature in a static field of 25 Oe, whereas field-cooled (FC) curves were obtained by cooling the samples in the same static field. The field dependence of the magnetization was measured up to 50 kOe, at $T = 5.0$ K, after zero-field cooling.

2.3. EXAFS and XANES Data Analysis. The program Viper[30] was used to sum the data, identify the beginning of the absorption edge, fit pre- and postedge backgrounds, and hence to obtain the normalized absorbance, χ, as a function of the modulus of the photoelectron wavevector k. The modular package DL_EXCURV,[31] based on the EXCURV98 code, was used in the final stage of data processing to model the experimental $\chi(k)$ in order to extract structural information. The fitting was carried out in k space up to a k value of 12 Å^{-1}. The structural parameters were obtained by nonlinear least-squares fitting in k-space with a k^3 weighting of the total experimental EXAFS spectra to emphasize the high-energy part of the spectrum. Fourier Transform (FT) of EXAFS data corrected for phase-shift shows peaks that correspond to local atom correlations. The positions of the peaks (R) correspond to bond distances between the central and the backscatterer atoms while the amplitudes are related to the coordination number (N) and to the static and thermal disorder (σ) of the atoms around the absorber. The errors in the fit parameters, R_i and $2\sigma_i^2$, were obtained from the 95% confidence level,[32] as calculated in DL_EXCURV. The S_0 parameter (called AFAC in EXCURV98), which is the many-body amplitude reduction factor, was determined to be 0.9 from fitting to the reference samples. The number of fitted parameters was always less than the number of statistically independent data points, as estimated in the standard way.[31]

The quality of the fit was judged from the normalized sum of residuals

$$R\ \text{factor} = \Sigma_n k_n^3 |\chi_{\text{expt}}(k_n) - \chi_{\text{fit}}(k_n)| / \Sigma_n k_n^3 |\chi_{\text{expt}}(k_n)| \times 100 \tag{1}$$

R factors were calculated on the experimental $k^3\chi(k)$ and R^* factors were calculated on the Fourier filtered $k^3\chi(k)$. The Fourier filtered $k^3\chi(k)$ is obtained by inverse transforming only the part of the Fourier transform (FT) corresponding to the shells which were fitted. The R^* factor is more meaningful in stating the goodness of the fit because the backtransforms exclude contributions that were not included in the fitting (i.e., contributions at low R due to imperfect background removal and contributions at high R due to large distance shells). Reasonable EXAFS fits of single shells typically have values of R factor around 20%; however, when the fit is performed on the total EXAFS spectra, higher values of R factor can still correspond to good fits especially if the fit is not extended to peaks at high R.

The XANES spectra were processed in the usual way to obtain normalized absorbance.[33] XANES at the K-edge involves the excitation of a 1s photoelectron into low-lying empty states at the central atom with p-type symmetry. The XANES have been analyzed using the "fingerprint" method, by comparing spectra from aerogels with those from reference cobalt and nickel silicate hydroxides compounds.

3. Results and Discussion

3.1. XRD. XRD patterns of the pure cobalt silicate hydroxide, ACo_450 and AFeCo_450 are reported in Figure 1A and those of pure nickel silicate hydroxide, ANi_450 and AFeNi_450 are presented in Figure 1B. Both reference compounds present two broad peaks at $2\theta \approx 35°$ and $2\theta \approx 60°$ along with other very weak peaks between $2\theta \approx 19°$ and $2\theta \approx 28°$. These peaks are typical of layered phyllosilicate-like structures. In particular, they correspond to the structure of $Co_3Si_2O_5(OH)_4$[34] and $Ni_3Si_2O_5(OH)_4$,[35] which are

---

(29) Decarreau, A. *Bull. Minéral.* **1980**, *103*, 579.

(30) Klementiev, K. V. *Appl. Phys.* **2001**, *34*, 209.

(31) Tomic, S.; Searle, B. G.; Wander, A.; Harrison, N. M. ; Dent, A. J. ; Mosselmans, J. F. W.; Inglesfield, J. E. *CCLRC Technical Report DL-TR-2005-001*; CCLRC: Warrington, 2005.

(32) *Error Report of the International XAFS Society Standards and Criteria Committee*; International XAFS Society: Camerino, Italy, 2000; http://ixs.iit.edu/subcommittee_reports/sc/.

(33) Bianconi, A. *X-ray Absorption: Principles, Applications, Techniques of EXAFS, SEXAFS and XANES*; Koningsberger, D. C., Prins, R., Eds; Wiley: New York, 1988; Chapter 11.

(34) PDF-2 card 21−0872.

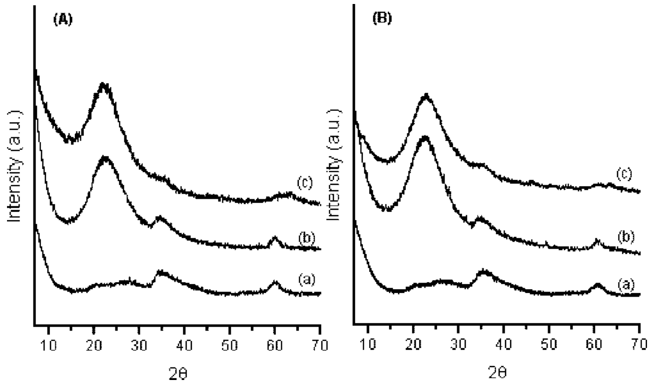

Figure 1. (A) XRD patterns of (a) $Co_3Si_2O_5(OH)_4$, (b) ACo_450, and (c) AFeCo_450; (B) XRD patterns of (a) $Ni_3Si_2O_5(OH)_4$, (b) ANi_450, and (c) AFeNi_450.

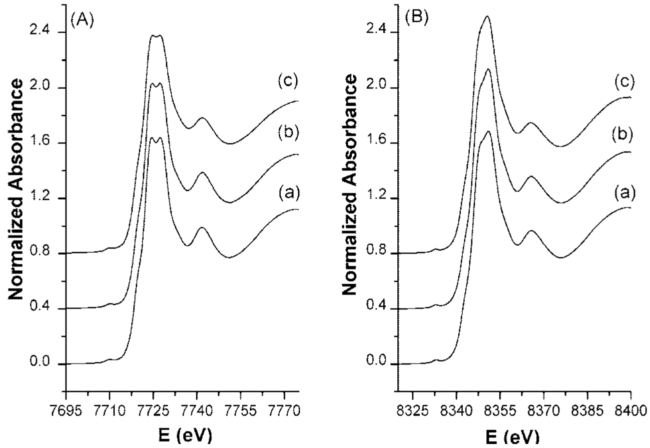

Figure 2. (A) XANES spectra of (a) $Co_3Si_2O_5(OH)_4$, (b) ACo_450, and (c) AFeCo_450; (B) XANES spectra of (a) $Ni_3Si_2O_5(OH)_4$, (b) ANi_450, and (c) AFeNi_450.

isostructural and belong to the Chrysotile subgroup. In the ACo_450 and ANi_450, the same two broad and weak peaks at $2\theta \approx 35°$ and $2\theta \approx 60°$ are observed as in the reference compounds, whereas in the region between 20° and 30° the halo due to the silica matrix is evident. In AFeCo_450 and AFeNi_450 the peaks at $2\theta \approx 35°$ and $2\theta \approx 60°$ are barely detectable because of the lower amount of Co and Ni and the additional presence of an iron-containing phase.

3.2. X-ray Absorption Spectroscopy. *3.2.1. XANES.* The XANES spectra at the Co K-edge for $Co_3Si_2O_5(OH)_4$, ACo_450 and AFeCo_450 are reported in Figure 2A and the spectra at the Ni K-edge for $Ni_3Si_2O_5(OH)_4$, ANi_450, and AFeNi_450 are reported in Figure 2B.

The spectra of $Co_3Si_2O_5(OH)_4$ and ACo_450 are practically identical, indicating the presence of the silicate hydroxide in the aerogel treated at 450 °C. The spectrum of AFeCo_450 is very similar and it is certainly very different from any other reference compound containing Co (i.e., Co, CoO, Co_3O_4, $CoFe_2O_4$, $Co(OH)_2$, see the Supporting Information).

The spectra of $Ni_3Si_2O_5(OH)_4$, and ANi_450 are again practically identical, demonstrating also in this case the formation of the silicate hydroxide in the aerogel. The AFeNi_450 is also very similar but presents slight differences in the prepeak shape and the main edge shape. The spectrum of AFeNi_450 is certainly not the same as other reference compounds containing Ni (i.e., Ni, NiO, $NiFe_2O_4$, see the Supporting Information).

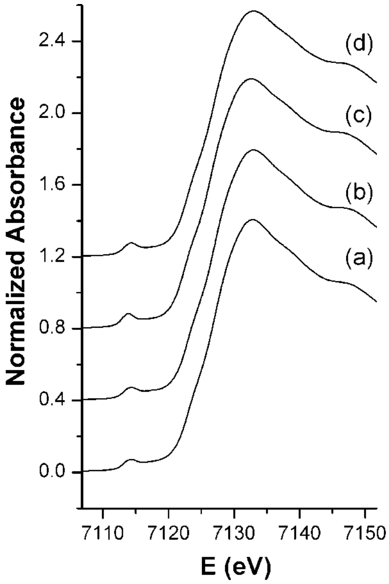

Figure 3. XANES spectra at the Fe K-edge of (a) ferrihydrite, (b) AFe_450, (c) AFeNi_450, and (d) AFeCo_450.

Spectra at the Fe edge reported in Figure 3 indicate that Fe is always present as ferrihydrite.

3.2.2. EXAFS. The EXAFS $k^3\chi(k)$ and the corresponding Fourier transforms at the Co K-edge for $Co_3Si_2O_5(OH)_4$, ACo_450, and AFeCo_450 are reported in panels A and B in Figure 4, respectively. The EXAFS $k^3\chi(k)$ and the corresponding Fourier transforms at the Ni K-edge for $Ni_3Si_2O_5(OH)_4$, ANi_450, and AFeNi_450 are reported in panels C and D in Figure 4, respectively. The frequencies of the oscillations of all the aerogels and those of the standards at both Co and Ni edges are very similar. However, the amplitudes of the oscillations of AFeCo_450 and AFeNi_450 are smaller than those of the aerogels containing only Co or Ni, which are very similar to those of the silicate hydroxide standards.

A detailed analysis was performed by fitting the EXAFS data at both Co and Ni edges. The results of the fitting are reported in Figure 4 as dotted lines. The starting N_i and R_i values in the fitting of the silicate hydroxide standards were taken from literature.[36,37] N_i values were kept fixed, whereas R_i values were left free to vary together with $2\sigma_i^2$ and ΔE_0. The same procedure has been used afterward for the aerogel samples.

The best fitting parameters at the Co K-edge are reported in Table 1. The first peak corresponds to a shell of 6 O at Co−O distance of 2.09 Å. The second peak is due to the overlap of two distances: a shell of 6 cobalt atoms at a distance of Co−Co 3.12 Å and a shell of 4 silicon atoms at a distance Co−Si of 3.27 Å. The Co−Co distance at 3.12 Å is typical of a edge-sharing layer of octahedra and the Co−Si

---

(35) PDF-2 card 22−0754.

(36) Schlegel, M. L.; Manceau, A.; Chateigner, D.; Charlet, L. *J. Colloid Interface Sci.* **1999**, *215*, 140.

(37) O'Day, P. A.; Rehr, J. J.; Zabinsky, S. I.; Brown Jr, G. E. *J. Am. Chem. Soc.* **1994**, *116*, 2938.

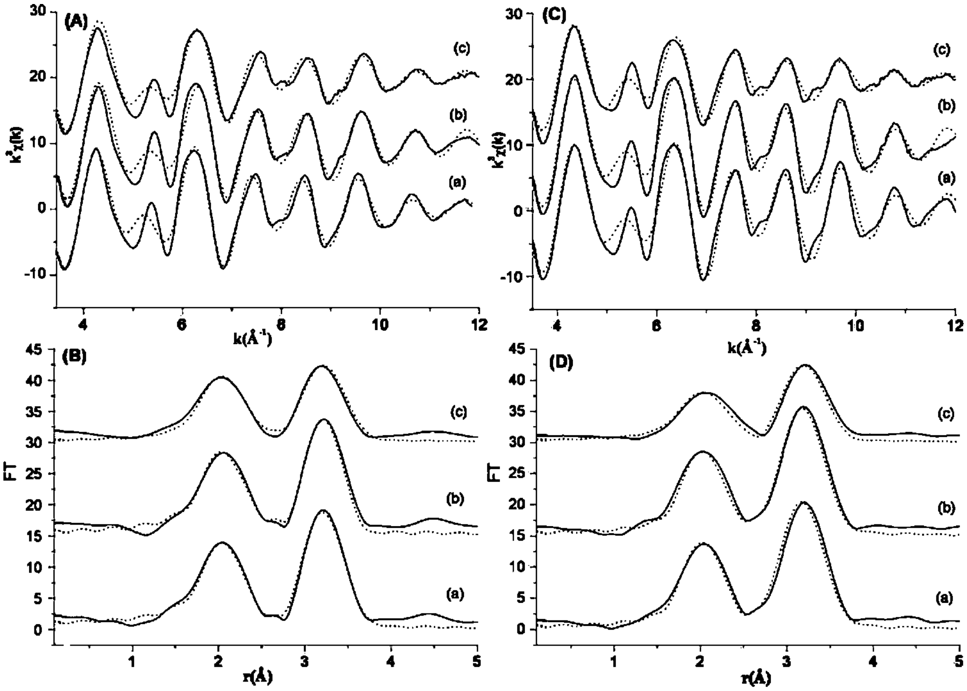

Figure 4. (A) EXAFS $k^3\chi(k)$ and (B) FT of (a) $Co_3Si_2O_5(OH)_4$, (b) ACo_450, and (c) AFeCo_450; (C) EXAFS $k^3\chi(k)$ and (D) FT of (a) $Ni_3Si_2O_5(OH)_4$, (b) ANi_450, and (c) AFeNi_450.

Table 1. Interatomic Distances (*R*) and Debye-Waller Factors (σ) Obtained by Fitting the Experimental EXAFS Interference Functions at Co K-edge of $Co_3Si_2O_5(OH)_4$, ACo_450, and AFeCo_450 (coordination numbers (*N*) were kept fixed, as reported in the text)

	Co K-Edge								
	$Co_3Si_2O_5(OH)_4$			ACo_450			AFeCo_450		
atom	*R* (Å)	*N*	$2\sigma^2$	*R* (Å)	*N*	$2\sigma^2$	*R* (Å)	*N*	$2\sigma^2$
O	2.09(1)	6	0.020(1)	2.09(1)	6	0.021(1)	2.09(1)	6	0.023(1)
Co	3.12(1)	6	0.017(1)	3.12(1)	6	0.021(1)	3.12(1)	6	0.025(1)
Si	3.27(1)	4	0.019(3)	3.27(1)	4	0.012(3)	3.27(1)	4	0.019(2)
		R factor = 24%			*R* factor = 26%			*R* factor = 26%	
		*R** factor = 18%			*R** factor = 17%			*R** factor = 16%	

Table 2. Interatomic Distances (*R*) and Debye−Waller Factors (σ) Obtained by Fitting the Experimental EXAFS Interference Functions at Ni K-Edge of $Ni_3Si_2O_5(OH)_4$, ANi_450, and AFeNi_450; (coordination numbers (*N*) were kept fixed, as reported in the text)

	Ni K-Edge								
	$Ni_3Si_2O_5(OH)_4$			ANi_450			AFeNi_450		
atom	*R* (Å)	*N*	$2\sigma^2$	*R* (Å)	*N*	$2\sigma^2$	*R* (Å)	*N*	$2\sigma^2$
O	2.07(1)	6	0.017(1)	2.07(1)	6	0.018(1)	2.08(1)	6	0.030(1)
Ni	3.07(1)	6	0.017(1)	3.07(1)	6	0.018(1)	3.07(1)	6	0.033(1)
Si	3.26(1)	4	0.014(3)	3.26(2)	4	0.012(2)	3.26(1)	4	0.013(3)
		R factor = 24%			R factor = 23%			*R* factor = 28%	
		*R** factor = 16%			*R** factor = 15%			*R** factor = 20%	

is typical of a layer of octahedra bridged to silicon tetrahedra by their corners.[27] The Co−Co distance at 3.12 Å is shorter than the Co−Co distance in $Co(OH)_2$ (3.17 Å) but longer than a fully crystallized clay (3.05−3.07 Å).[7]

The best fitting parameters at the Ni K-edge are reported in Table 2. The first peak corresponds to a Ni−O distance of 2.07 ± 0.01 Å with a first coordination shell of 6 oxygens. The second peak, due to the overlap of two distances, was fitted with a shell of 6 nickel atoms at a distance of Ni−Ni 3.07 Å and a shell of 4 silicon atoms at a distance Ni−Si of 3.26 Å.

Distance and coordination parameters found at the Co and Ni edges are typical of $Co_3Si_2O_5(OH)_4$ and $Ni_3Si_2O_5(OH)_4$, respectively. It is evident that the phases $Co_3Si_2O_5(OH)_4$ and $Ni_3Si_2O_5(OH)_4$ are present in the aerogels containing only cobalt or nickel and also in the mixed aerogels containing Fe/Co and Fe/Ni.

The EXAFS analysis at Fe K-edge is reported in Figure 5 and Table 3. Because the structure of ferrihydrite is not well-known, we decided to use the coordination numbers (*N*) and interatomic distances (*R*) found in a previous EXAFS paper as starting values for the fitting,[38] which was carried out letting distances free to vary along with $2\sigma_i^2$ while coordination numbers were kept fixed. The EXAFS analysis at Fe K-edge confirms that the iron is present in form of ferrihy-

---

(38) Drits, V. A.; Sakarov, B. A.; Salyn, A. L.; Manceau, A. *Clay Miner.* **1993**, *28*, 185.

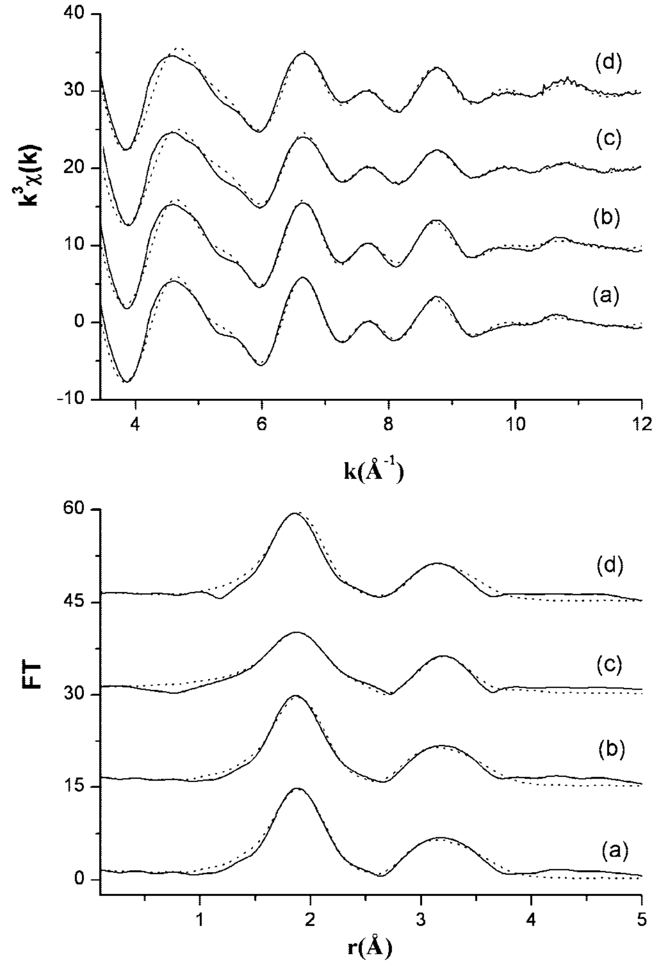

Figure 5. EXAFS $k^3\chi(k)$ and FT at the Fe edge of (a) ferrihydrite, (b) AFe_450, (c) AFeNi_450, and (d) AFeCo_450 from experimental (continuous line) and fit results (dotted line).

drite. Therefore, two separate phases are present: Co and Ni are in the form of silicate hydroxide and iron is present in form of ferrihydrite. This result shows that Co and Ni have a higher affinity for silica than Fe. The affinity of Co and Ni for silica has been proved in many previous works, for example, Manceau et al.[26] reported the evidence of formation of Co rich hydrous phases similar to $Co_3(Si_2O_5)(OH)_4$ and $Co_3(Si_2O_5)_2(OH)_2$ by sorption of Co on quartz.

It is interesting to observe that very similar cobalt and nickel phases have been obtained adding cobalt or nickel nitrate to amorphous silica using urea as generator of hydroxyl.[16] On the other hand, no similar clay-like structures have been observed in similar systems prepared in our laboratory using an all-acidic one-step sol−gel process.[17,39] In the current two-step sol−gel process, the urea is used on prehydrolyzed TEOS. Therefore, it is possible that Co and Ni are absorbed on the surface of silica particles already formed in solution. This would be supported by studies in which metal cations such as Mg, Co and Ni form layered structures when they are absorbed on a silica surface or more generally when are in contact with silicates. In fact, even in soils and sediment, quartz is often coated by layered minerals. However, the mechanism of formation of the layered structures is not clear. It could precipitate homogeneously from solution or heterogeneously on a silica or silicate surface.[26]

3.3. Electron Microscopy. In Figure 6 are reported the TEM bright-field images of $Co_3Si_2O_5(OH)_4$, ACo_450, and AFeCo_450, $Ni_3Si_2O_5(OH)_4$, ANi_450, and AFeNi_450 samples. The images of both $Co_3Si_2O_5(OH)_4$ and $Ni_3Si_2O_5(OH)_4$ reference compounds show dense material with no obvious porosity or nanostructure, which is consistent with bulk phases. (The layered structure within phyllosilicates cannot be seen in low-resolution TEM images.)

In all the aerogel samples, the TEM images clearly show the extended porosity typical of the aerogels. In addition, nanoparticles with apparently one-dimensional shape can be evidenced. These can be attributed to the presence of Co and Ni phyllosilicate nanoparticles because they are present in ACo_450 and ANi_450, whereas they are absent in AFe_450 (see the Supporting Information). The anisotropic nanostructures are very abundant in ACo_450 and ANi_450 samples but are also detectable in AFeCo_450 and AFeNi_450 samples. The typical dimensions of the anisotropic nanostructures in ACo_450 and ANi_450 samples is a few nanometers wide and several 10s nm long. The nanostructures are longer in ANi_450 compared to ACo_450. The one-dimensional appearance of these nanostructures could arise from two different shapes: (i) a needlelike (acicular) shape, or (ii) a disk- or sheetlike shape that is always “edge-on” to the beam. The number of atoms in the path of the electron beam in (i) would be uniform along the length of the nanoparticle, whereas that in (ii) would be less at the ends and greater in the middle of the nanoparticle. Hence the image contrast from the nanoparticle in (i) should be uniform along its length, whereas in (ii) it should be less at the ends and greater in the middle of the nanoparticle. It is difficult to judge from the TEM images whether (i) or (ii) occurs.

The VG501 STEM microscope (with very small 0.13 nm probe) was used to collect high-resolution bright-field images of AFeCo_450 and AFeNi_450 samples, which are shown in Figure 7. In these images, anisotropic nanostructures are visible again, having a one-dimensional appearance. The STEM images were obtained by scanning the 0.13nm probe over the sample, and the image contrast reflects the number of atoms in the electron beam. Because the image contrast of the nanoparticles seems uniform along their length, this suggests that (i) the nanoparticles have a needle-like (acicular) shape, which we refer to as nanoneedles. Alternatively, (ii) a disk- or sheetlike shape edge-on to the beam could be expected to appear lighter at the ends and darker in the middle, which does not seem to be the case. The typical size of the anisotropic nanostructures in AFeCo_450 and AFeNi_450 samples is ∼1 nm wide and 10−20 nm long. There is also evidence of a layered structure. The interlayer spacing was estimated by taking profiles of the image intensity from the regions indicated by rectangles. The estimated interlayer spacing was 0.33 ± 0.02 nm for the AFeCo_450 sample and 0.31 ± 0.02 nm for the AFeNi_450 sample. This does not correspond to any known interlayer spacing in ferrihydrite (which has a largest planar spacing of $d_{100} = 0.250$ nm), but

---

(39) Casula, M. F.; Corrias, A.; Paschina, G. *J. Mater. Chem.* **2002**, *12*, 1505.

Table 3. Interatomic Distances (*R*) and Debye−Waller Factors (*σ*) Obtained by Fitting the Experimental EXAFS Interference Functions at Fe K-Edge of Ferrihydrite, AFe_450, AFeNi_450, and AFeCo_450; (coordination numbers (*N*) were kept fixed, as reported in the text)

	Ferrihydrite			AFe_450			AFeNi_450			AFeCo_450		
atom	*R* (Å)	*N*	$2\sigma^2$	*R* (Å)	*N*	$2\sigma^2$	*R* (Å)	*N*	$2\sigma^2$	*R* (Å)	*N*	$2\sigma^2$
O	1.96(1)	5.1	0.023(1)	1.95(1)	5.1	0.023(1)	1.95(1)	5.1	0.028(2)	1.95(1)	5.1	0.024(1)
Fe	2.87(1)	0.8	0.020(1)	2.87(1)	0.8	0.020(1)	2.87(1)	0.8	0.016(3)	2.87(3)	0.8	0.020(1)
Fe	3.03(1)	2.4	0.019(1)	3.03(1)	2.4	0.019(1)	3.04(1)	2.4	0.019(2)	3.04(1)	2.4	0.019(1)
Fe	3.45(1)	1.5	0.018(1)	3.45(1)	1.5	0.018(1)	3.42(2)	1.5	0.024(1)	3.42(1)	1.5	0.020(2)
	R factor = 19%			*R* factor = 21%			*R* factor = 22%			*R* factor = 24%		

is roughly similar to the interlayer spacing in $Co_3Si_2O_5(OH)_4$ and $Ni_3Si_2O_5(OH)_4$ of $d_{002} = 0.360$ nm.

3.4. Magnetic Measurements. Panels A and B in Figure 8 show the ZFC and FC curves of the samples containing cobalt and nickel, respectively. All the ZFC static magnetization curves show a well-defined maximum at the temperature T_{max}. Such observed irreversibility is due to the characteristic blocking−unblocking process of the particle magnetic moment when thermal energy is changed. As the relaxation time of a magnetic particle increases with decreasing temperature, we can define, for a certain observation time, a characteristic temperature, called blocking temperature, below which the particle moment appears blocked with respect to the time scale of the experiment. At the blocking temperature (T_B), the thermal energy k_BT overcomes the energy barrier for the magnetic moment reversal associated with the total anisotropy energy. At temperatures higher than T_B, the magnetization in the presence of a magnetic field reaches its thermal equilibrium value, mimicking an atomic paramagnet. Because the magnetic moment of the single particle is much higher than the atomic one, the magnetic state for $T > T_B$ is called superparamagnetic. In this state, the remanence and the coercivity of the system vanish.[40] The blocking temperature and anisotropy constant that are measured have to be considered as effective, mean values, as they result from measurements on the entire nanoparticle ensemble. As usually reported, the blocking temperature T_B is assumed to be equal to that where the ZFC curve shows a maximum (T_{max}). Such a temperature is related in a complex way both to the effective magnetic anisotropy constant, K_{eff}, of the sample and to the mean nanoparticle volume, $\langle V \rangle$. K_{eff} contains all the contributions that come from magnetocrystalline surface, shape, and stress anisotropy. Usually, as a first approximation, T_{max} is considered proportional to the product $K_{eff} \times \langle V \rangle$.[41] The temperature at which the ZFC and FC curves split (T_{irr}), corresponds to the deblocking of magnetic moment of the particles largest in size. Consequently, the difference between T_{max} and T_{irr} gives an indication of the narrowness of anisotropy energy barrier distribution of the particles.

The values of T_{max} and T_{irr} of all the samples are reported in Table 4, together with all the parameters obtained by the hysteresis loops, which are shown in panels A and B in Figure 9. First, the T_{max}, together with the coercive field H_c of each sample, increases going from the pure silicate hydroxides to the aerogels. This is not surprising if we consider that TEM analysis clearly shows that the pure silicate hydroxides are not in nanometric form. On the contrary, in all the aerogel samples, the silicate hydroxides are made of anisotropic nanostructures that appear to be in

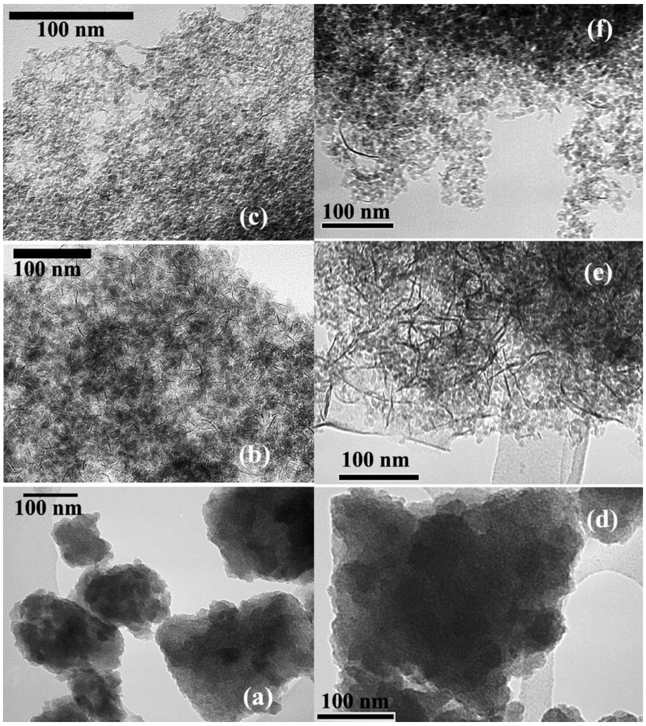

Figure 6. TEM bright-field images of (a) $Co_3Si_2O_5(OH)_4$, (b) ACo_450, (c) AFeCo_450, (d) $Ni_3Si_2O_5(OH)_4$, (e) ANi_450, and (f) AFeNi_450.

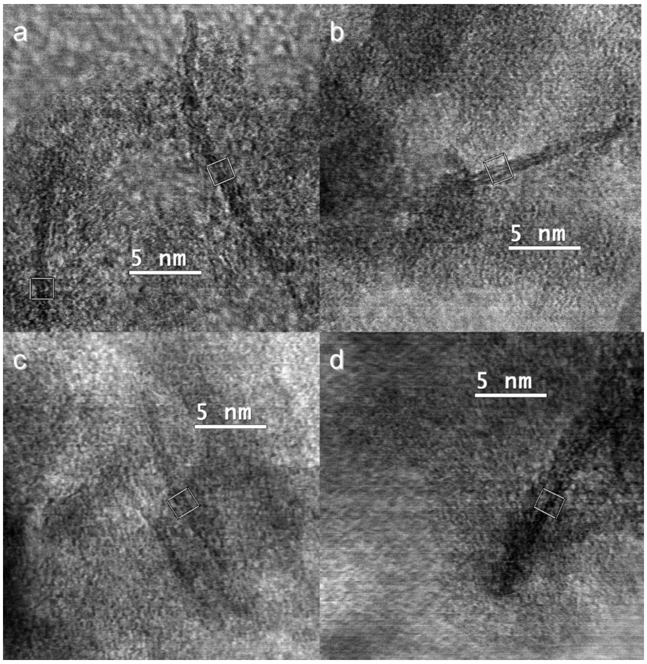

Figure 7. High-resolution BF STEM images of (a, b) AFeCo_450 and (c, d) AFeNi_450 samples. Anisotropic nanostructures are visible, and there is evidence of layered structure. Rectangles show where the interlayer spacing was estimated from the profile of image.

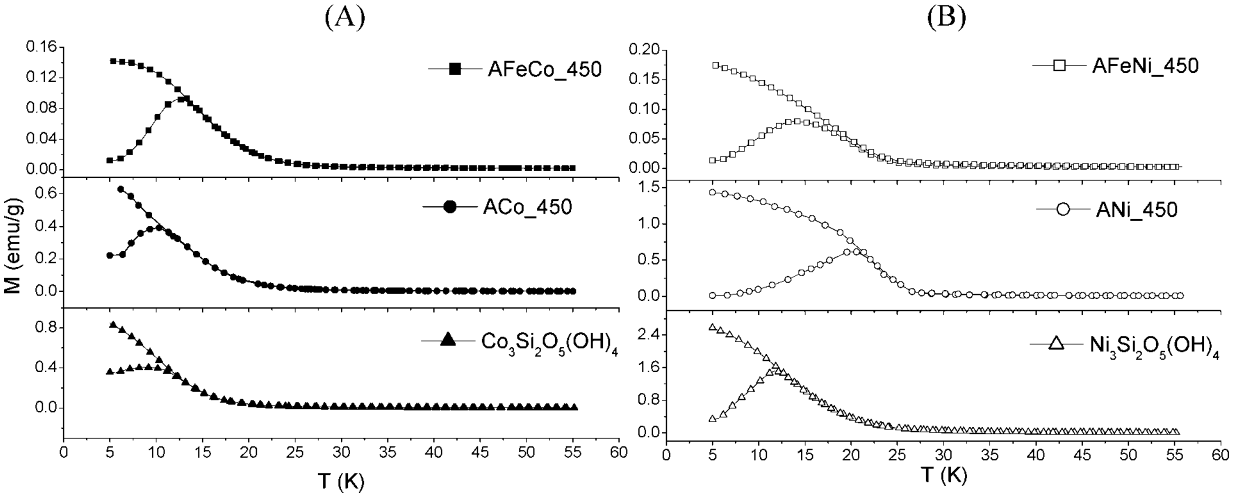

Figure 8. ZFC and FC magnetizations curves, obtained with $H = 25$ Oe, of (A) AFeCo_450, ACo_450, and $Co_3Si_2O_5(OH)_4$ samples; (B) AFeNi_450, ANi_450, and $Ni_3Si_2O_5(OH)_4$ samples. The corresponding parameters (T_{max} and T_{irr}) are reported in Table 4.

Table 4. Magnetic Parameters (T_{max}, T_{irr}, H_C, M_R, M_{5T}, M_R/M_{5T}) of AFeCo_450, ACo_450, $Co_3Si_2O_5(OH)_4$ and AFeNi_450, ANi_450, $Ni_3Si_2O_5(OH)_4$ Samples, as Determined by the Measurements Reported in Figures 8 and 9

sample	T_{MAX} (K)	T_{irr} (K)	H_C (Oe)	M_R (emu/g)	M_{5T} (emu/g)	M_R/ M_{5T}
$Co_3Si_2O_5(OH)_4$	9	14	101	3.9	56.5	0.07
ACo_450	10	13	324	2.5	13.6	0.18
AFeCo_450	13	52	635	1.4	6.6	0.21
$Ni_3Si_2O_5(OH)_4$	12	22	724	12.4	54.1	0.23
ANi_450	20	30	2350	4	11.6	0.35
AFeNi_450	14	40	1265	0.8	5.2	0.15

the form of nanoneedles or nanosheets, and this greatly influences their magnetic behavior, mainly because both the surface and shape contribution to the magnetic effective anisotropy increase.

Moreover, some differences in the variation of magnetic behavior is observed between the aerogels containing cobalt and the ones containing nickel. In fact, going from ACo_450 to AFeCo_450, the coercive field increases of a factor 2, whereas when going from ANi_450 to AFeNi_450, the coercive field decreases. The TEM investigation shows that in both ACo_450 and AFeCo_450 samples, the cobalt silicate hydroxide is present in the form of nanoneedles (or nanosheets) with similar sizes; therefore, the increase in coercivity cannot be ascribed to a different shape and surface contribution to the effective magnetic anisotropy. Besides, TEM analysis also reveals that the typical distance among the acicular particles of cobalt silicate hydroxide is not very different in the two samples, and the hysteresis loops indicate that the mean nanoparticle magnetic moment are also unaffected. As a consequence, a modification in the strength of dipolar magnetic interactions (likely present) among the particles can also be ruled out.[42] Therefore, the increase in coercivity might be due to the presence of ferrihydrite, in consideration of its high ($K_{eff} \approx 3 \times 10^6$ erg cm^{-3}) magnetocrystalline anisotropy value.[43] There is another possible explanation of such behavior, i.e., if a small amount of iron ions substitute cobalt in the lattice of the silicate hydroxide, this would give rise to an expected harder magnetic phase, i.e., a phase with a higher magnetocrystalline anisotropy.[44,45]

The increase in the effective anisotropy of AFeCo_450 is further confirmed by the corresponding small increase in the M_R/M_{5T} ratio, which indicates that at the temperature of 5 K, a larger fraction of magnetic particles is still blocked at zero external magnetic field compared to the fraction in the ACo_450 sample.

A similar explanation can be invoked also for the variation in the magnetic behavior in the samples containing nickel. In going from the ANi_450 to the AFeNi_450 sample, decreases in the coercive field, T_{max}, and the M_R/M_{5T} ratio were observed. In this case, if a small amount of nickel ions are substituted by iron in the lattice of the silicate hydroxide, the magnetocrystalline anisotropy is expected to become quite lower.[46] Also, in the AFeNi_450 sample, ferrihydrite is present, which should give rise to an increase in the effective anisotropy, because the magnetocrystalline anisotropy of ferrihydrite is higher than that of the nickel silicate hydroxide. Therefore, the observed decrease in the effective anisotropy indicates that the effect of the diffusion of iron in the nickel silicate hydroxide lattice must be largely dominant in decreasing the total anisotropy, and all the related parameters decrease consequently. The diffusion of Fe into the silicate hydroxide phase should be quite limited because the EXAFS and XANES results at the Fe K-edge of the AFeCo_450 and AFeNi_450 are very similar to those of AFe_450 sample, but even a small diffusion of Fe could be enough to affect the magnetic properties.

It is possible to observe that going from ACo_450 to AFeCo_450 and from ANi_450 to AFeNi_450, a decrease in M_{5T} is found and the magnetization becomes further from the saturation. This is not surprising if we consider that (i) the ACo_450 and ANi_450 samples have a much

---

(40) Néel, L. *Ann. Geophys.* **1949**, *5*, 99.
(41) Kneller, E. F.; Luborsky, F. E. *J. Appl. Phys.* **1963**, *34*, 656.
(42) Dormann, J. L.; Bessais, L.; Fiorani, D. *J. Phys. C: Solid State Phys.* **1988**, *21*, 2015.
(43) Duarte, E. L.; Itri, R.; Lima, Jr, E.; Baptista, M. S.; Berquó, T. S.; Goya, G. F. *Nanotechnology* **2006**, *17*, 5549.
(44) Casu, A.; Casula, M. F.; Corrias, A.; Falqui, A.; Loche, D.; Marras, S. *J. Phys. Chem. C* **2007**, *111*, 916.
(45) Shenker, H. *Phys. Rev.* **1957**, *107*, 1246.
(46) Caruntu, G.; Dumitru, I.; Bush, G. G.; Caruntu, D.; O'Connor, C. J. *J. Phys. D: Appl. Phys.* **2005**, *38*, 811.

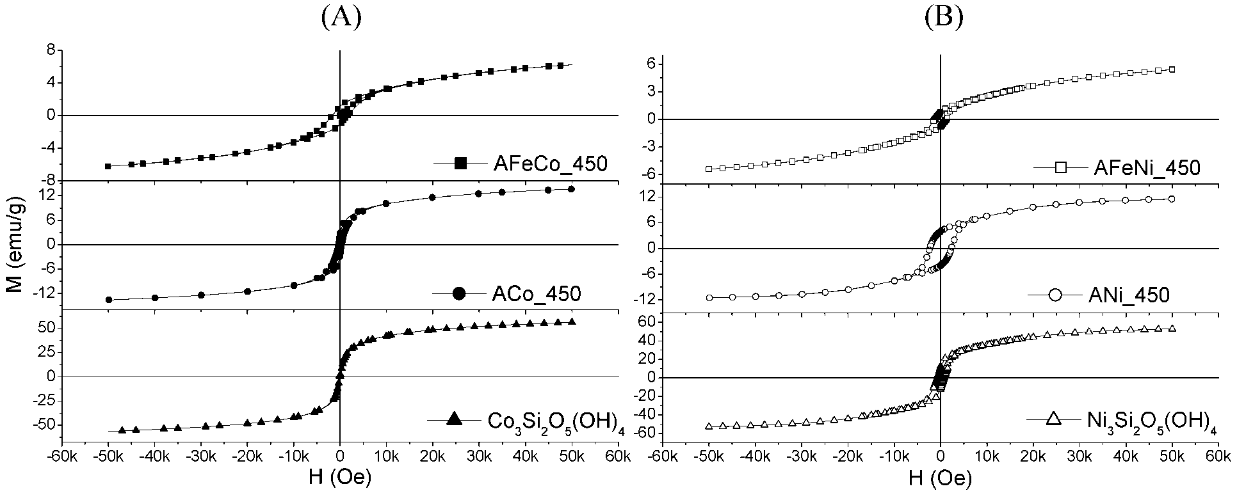

Figure 9. Low-temperature ($T = 5$ K) ZFC magnetic hysteresis loops of (A) AFeCo_450, ACo_450, and $Co_3Si_2O_5(OH)_4$ samples; (B) AFeNi_450, ANi_450, and $Ni_3Si_2O_5(OH)_4$ samples. The corresponding parameters (H_C, M_R, M_{5T}, M_R/M_{5T}) are reported in Table 4.

higher content of Co and Ni, and therefore of the silicate hydroxide phase, with respect to the AFeCo_450 and AFeNi_450 samples; (ii) the presence of ferrihydrite gives an additional contribution to the total magnetization of the latter two samples, the M_{5T} of pure ferrihydrite being equal to 11 emu/g (see the Supporting Information), which is around 5 times lower than those of both pure cobalt and nickel silicate hydroxide. Finally, the presence of ferrihydrite is the most likely cause for the fact that the magnetization becomes further from saturation in the AFeCo_450 and AFeNi_450 samples with respect to ACo_450 and ANi_450 samples. In fact, ferrydrite is very far from saturation even at a field of 5 T (see the Supporting Information).

It should be pointed out that a magnetic behavior quite similar to our samples was observed in $Co-SiO_2$ aerogels.[47] However, in that case, the magnetic results were attributed to the presence of Co and CoO, even if evidence was found for the presence of a cobalt silicate hydroxide. That study did not include X-ray absorption spectroscopy, which would provide clear information on the environment of Co as seen in the present study. Our results, which have been extended to the pure silicate hydroxides, indicate without any doubt that the observed magnetic behavior is due to the silicate hydroxides.

5. Conclusions

The study of aerogels containing iron and cobalt or iron and nickel dispersed into silica and submitted to calcination at 450 °C, which are intermediates in the sol−gel preparation of $CoFe_2O_4-SiO_2$ and $NiFe_2O_4-SiO_2$ nanocomposites, was performed using XRD, TEM, STEM, EXAFS, XANES, and magnetic measurements. The comparison with the data from aerogels prepared without Fe and with those from pure cobalt and nickel silicate hydroxides, prepared as reference compounds, indicates that iron on the one hand, and cobalt or nickel on the other hand, are present in separate phases dispersed into the silica matrix. The presence of iron in the form of ferrihydrite, a poorly crystalline iron oxide hydroxide, already suggested by previous studies, was confirmed. The presence of another phase of either Co or Ni silicate hydroxides was clearly evidenced from the comparison of the XANES and EXAFS data of the aerogels with the data of the pure Co and Ni silicate hydroxides. These compounds, which have a clay like structure, are present in the aerogels in the form of anisotropic nanostructures with a one-dimensional appearance, as evidenced by TEM. High-resolution STEM images showed evidence of a layered structure within anisotropic nanostructures, with estimated interlayer spacing of 0.32 ± 0.02 nm, roughly similar to that in Co and Ni silicate hydroxides.

The magnetic measurements confirm that the nanoneedles or nanosheets observed in the samples containing only cobalt or nickel are composed of the corresponding silicate hydroxide. However, mainly as a consequence of their nanosize and shape, an important variation in coercivity is observed for the silicate hydroxide in the aerogels with respect to the bulk silicate hydroxide samples. Furthermore, in the samples prepared using iron with cobalt or iron with nickel, two main concomitant effects were observed: the contribution to the total magnetic behavior due to the presence of ferrihydrite, and possibly a slight diffusion of iron into the silicate hydroxide nanoparticles.

Supporting Information Available: XANES spectra of Co and Ni reference compounds, TEM image of the AFe_450 aerogel sample, and hysteresis loops of ferryhydrite (PDF). This material is available free of charge via the Internet at http://pubs.acs.org.

Acknowledgment. The authors thank XAFS (Elettra) beamline scientists Luca Olivi and Andrea Cognigni for assistance during data collection. D.L. thanks the Banco di Sardegna for a research grant. This work was supported by a European Community Sixth Framework Programme Marie Curie Intra-European Fellowship (Contract MEIF-CT-2005-024995) and by the EPSRC UK for access to the SuperSTEM (Grant EP/F03699X/1).

CM8029714

---

(47) Dutta, P.; Dunn, B. C.; Eyring, E. M.; Shah, N.; Huffman, G. P.; Manivannan, A.; Seehra, M. S. *Chem. Mater.* **2005**, *17*, 5183.